Supplement of Atmos. Chem. Phys., 23, 6357–6382, 2023
https://doi.org/10.5194/acp-23-6357-2023-supplement

Atmospheric Chemistry and Physics
Open Access
EGU

Supplement of

Development of a CMAQ–PMF-based composite index for prescribing an effective ozone abatement strategy: a case study of sensitivity of surface ozone to precursor volatile organic compound species in southern Taiwan

Jackson Hian-Wui Chang et al.

Correspondence to: Neng-Huei Lin (nhlin@cc.ncu.edu.tw)

Supplementary Materials

Photochemcial Assessment Monitoring Stations (PAMS)

Taiwan's Environmental Protection Adminstrations (Taiwan EPA) has set up nine Photochemical Assessment Monitoring Stations (PAMS) in western Taiwan, each was placed to the nearby air quality monitoring station to enable simulatenous measurement of air pollutants and VOC species. Among the nine PAMS stations, three stations are located in southern Taiwan namely Chaozhou (CZ, 22.52°N, 120.56°E), Qiaotou (QT, 22.76°N, 120.64°E), Xiaogang (XG, 22.57°N, 120.34°E). The CZ station is in a suburban area which is near to a freeway and an expressway both on the west side, with some small factories scattered around. The QT station is near to a freeway with an expressway to the east, with three industrial parks to the northwest, south and south-southeast. It also hosted a major oil refinery in the south-southeast industrial park. The XG station is surrounded by a freeway on the northwest side, a harbor to the northwest and four industrial parks to the east, southeast and west.

The Taiwan EPA VOC data sampling and instrumental analysis adopted the standards same as those used by the US EPA. Each PAMS station collected 54 VOC species on hourly basis, including 28 alkanes, 9 alkenes, 1 alkyne, 16 aromatics. The VOC species are monitored by a commercial GC system and the instruments are calibrated using standard gas every five days using calibration curves, relative standard deviation (RSD), and method detection limit (MDL) for each VOC species. To ensure high quality assurance and quality control QA/QC data, the calibration curve has correlation coefficient >0.995; the precision was determined by seven replicate measurements of the calibration gas and the RSD less than 10% is maintained for each VOC species. All of the October 2018 PAMS-QA/QC data at CZ, QT and XG station were used in this study

Model Evaluations

First, we assessed the WRF model's ability to reasonably reproduce the meteorology conditions. 2-m temperature (T2), 10-m wind speeed (WS) and wind direction (WD) measured by the 15 air quality Taiwan Environmental Protection Agency (TEPA) stations were compared with WRF model output at the corresponding grid cell for each stations for the entire simulation period 7-22 Oct 2018 (Figure S11). The model evaluation metrics averaged from the

15 stations are shown in Table S2. Among the 15 stations, 10 stations are selected to represent the urban stations and the other 5 stations as rural stations (Table S3). The comparison shows that the simulations captured the observed diurnal maxima and minima of T2 and WS accurately for both urban and rural stations. The 2-m temperature is slighly underestimated by 0.92 °C, but still highly correlated with the measured T2 with IOA > 0.89. For wind speed, the mean bias (MB, 0.15 m s^{-1}), mean average gross error (MAGE, 0.96 m s^{-1}), index of agreement (IOA, 0.85) are presented. For wind direction, the wind normalized mean bias (WNMB) and wind normalized mean error (WNME) are -1.12 °, 28.26 °, respectively. The relatively uniform comparison show that the WRF simulation agrees well with the observed wind directions.

The comparison between the observed and simulated timeseries O_3, NO_2 and VOC from various TEPA stations are prsented in Figure S12. In general, the air quality modelling system produces a good simulation of the diurnal variations in O_3. The magnitude of the daily 8h maxima and the spatial distribution for O_3 are also reasonably well predicted where higher concentration is simulated over the western coastal region and gradually decreases along the mountainous region and low concentration over the eastern coastal region (Figure S13a). Based on the modelled result, the occurrence of daily 8h maxima O_3 > 75 ppb is less frequent over the urban area nearby the large point source but more frequently occurs over the inland area, indicating the severity of the inland photochemical ozone pollution problem in the study area (Figure S13b). The model performance for NO_2 and VOC are also evaluated in Table S2. The mean normalized bias (MNB) of NO_2 and VOC are estimated as 28% and -0.42%, respectively, which is comparable to the acceptable performance range of -40 to 50% recommended by USEPA benchmark. The simulated NO_2 and VOC are also well correlated with the observed value with IOA greater than 0.67 and 0.63, respectively. The spatial distribution of the modelled daily maxima NO_2 and VOC are also highly concentrated over the western coastal urban area with abundant emission sources. In overall, the statistical performance for modelled O_3, NO_2 and VOC are acceptable and comparable to other models and studies (Cheng et al., 2015; Li et al., 2013; Tang et al., 2017; Tsai and Wu, 2006).

Zero-out Source Contribution

We further examine the relationship between ozone and its precursors (i.e. NO_x and VOC) by decomposing the zero-out source contribution of domain-wide NO_x and VOC emissions to ozone concentration in the cells corresponding to urban area (represented by urban grid cells) and inland area (represented by cropland/woodland mosaic). Defined by (Cohan et al., 2005), the zero-out source contribution of a source species or region p_j, representing the reduction in concentrations that would occur if that source was removed completely, can be approximated by:

$$ZOC(p_j) \approx S_j^{(1)} - \frac{1}{2} S_{j,j}^{(2)} \tag{10}$$

In the case for estimating ozone reduction due to NO_x and VOC, the contribution of the two sources p_{NOx} and p_{VOC} can be approximated by

$$ZOC(p_{NOx} + p_{VOC}) \approx \left(S_{NOx}^{(1)} - \frac{1}{2} S_{NOx,NOx}^{(2)} \right) + \left(S_{VOC}^{(1)} - \frac{1}{2} S_{VOC,VOC}^{(2)} \right) - S_{Nox,VOC}^{(2)} \tag{11}$$

which incorporates the first-order, second-order and cross sensitivity of NO_x and VOC. The first two terms represents the zero-out contribution of NO_x emissions; the third and forth terms represents the zero-out contribution of VOC emissions and finally the cross sensitivity between NO_x and VOC emissions represents the extent to which each emitter influences the zero-out contribution of the other.

On the zero-out contribution basis, NO_x emissions are more important than the VOC emissions (Figure S14). Unlike the previous studies in Atlanta (Cohan et al., 2005) and Houston (Xiao et al., 2010) that demonstrated a clear daily cycle of NO_x first- and second-order zero-out contributions (i.e. positive during daytime; negative during nighttime), our results show the NO_x first-order zero-out contribution remains largely negative (increase of O_3) even during the daytime photochemical active hours in both urban and inland areas indicating the important role of titration effect on ozone. This is likely attributed to the high NO_x emissions of the study area where the total emission averaged during the entire simulation is approximately 807 tones per day (tpd) in urban area (653 km^2) and 187 tpd in inland area (459 km^2) which gives emission denisty 1.236 tpd/km^2 and 0.407 tpd/km^2, respectively that is far greater than Atlanta and Houston (Table S4). Besides, inland ozone experiences higher second-order NO_x contribution especially daytime

when compared to urban. The intense non-linearity of NO_x zero-out contribution in inland areas indicated by the large negative second-order sensitivities can be explained by the inland ozone production sensitivity favors of NO_x-limited regime. First-order VOC zero-out contribtion in both urban and inland areas is always positive (decrease in O_3) and becomes important only during the daytime hours, reflecting the dominant effect of OH free radicals in driving the HO_x cycle. Note that the peak of first-order VOC contribution in inland area is slightly shifted or delayed 1-2 hours as compared to urban areas. This temporal shift is possibly attributed to the sea-breeze penetration that pushes the urban polluted air (i.e. anthropogenic VOC) towards inland areas. The cross-sensitivity between NO_x and VOC zero-out contribution is always negative (increase of O_3) in both urban and inland areas, indicating that when NO_x (VOC) emissions are reduced, ozone becomes less sensitive to VOC (NO_x). Due to the more intense non-linearity NO_x contribution in inland areas than urban areas, the inland cross-sensitivity is also found to be higher than urban areas. Rural areas far from anthropogenic emissions typically exhibited more linear response to NO_x and virtually no response to VOC. However, our modelling indicates the inland areas' ozone response to VOC zero-out contribution remain largely dominant and also has high non-linearity of NO_x contribution. This tells us that VOC control can achieve the co-benefit to reduce the ozone pollution problem in both urban and inland area.

Source Profiles of PMF Model

Factor 1 is dominated by single-species isoprene which is indicative of the biogenic emissions. It is accounted for 90.9%, 83.4%, and 80.9% in CZ, QT, and XG, respectively. The hourly factor contribution also displays a clear diurnal cycle peak at the noon time 10-12 LST in all three stations (Figure 10). The contribution of biogenic sources to total VOCs concentration is 12%.

Factor 2 is dominated by aromatic-species with high percentage of toluene (32.2% in CZ, 59.4% in QT, 62.5% in XG), ethylbenzene (51.4% in CZ, 40.0% in QT, 35.4% in XG), m,p-xylene (64.5% in CZ, 40.6% in QT, 35.9% in XG), and o-xylene (66.2% in CZ, 42.1% in QT, 41.2% in XG) in all three stations. It is also characterized by moderate percentage of C6-C8 alkanes and benzene. A high portion of BTEX is typically related to the use of solvents in painting, coating, synthetic fragances, adhesives and clearning agents (Huang and Hsieh, 2020; Hui et al., 2018; Wu

et al., 2016). The hourly factor contribution in XG has a clear bimodal peak at 10 and 16 LST, both correspond to industrial activity. The contribution of solvent usage to total VOCs concentration is 17%, which is the third most important source of VOC pollution in the study area.

Factor 3 is mainly dominated by alkanes-species with high percentage of ethane (45.6%), propane (53.0%), isobutane (51.4%) and n-butane (52.1%) in all three stations. It also features lower percentages of C6-C10 alkanes and aromatics. These species are closely related to vehicular emissions (Hui et al., 2018; Liu et al., 2008). Besides, moderate percentage of isopentane (32.3%) and n-pentane (34.3%) are also observed in this factor, which are the major indicators of gasoline fuel evaporation (Li et al., 2018). Acetylene is a well-known combustion tracer and also presented in this source, indicating that the emission exhaust is likely related to liquefied petroluem gas (LPG) emissions. The contribution of vehicular emissions to total VOC concentration was 22%, which constituted the largest source of VOC pollution in the study area. This is also consistent with findings from Huang and Hsieh (2020) where traffic emissions including vehicular emissions and vehicle fuel evaporation has the largest proportion in western Taiwan, accounted for 23-37% of the total contributions.

Factor 4 is dominated by a single-species cyclohexane, accounted for 76.0% in CZ, 68.6 % in QT, and 77.5 % in XG. Cyclohexane is usually used in the production of intermediates for plastics, textile and nylon, which has a variety of common applications such as clothing, tents, carpets and thermoplastics. These intermediates are cyclohexanol and cyclohexanone, which in turn are use mainly as precursors for the production of adipic acid and caprolactam. The hourly factor contribution in QT and CZ has a clear diurnal cycle peak in the noon time at 11 and 13 LST, respectively which correspond to industrial activity. A two-hours lag in CZ seems to indicate that the source is mainly originated from QT where it is located at the urban coastal region, and subsequently transported to inland CZ downwind of the northeasterly wind. In contrast, the hourly factor contribution in XG peaks in the early morning hours 03-06 LST. These hours are unlikely related to the industrial activity and we speculated it is due to the entrainment process that injects the remaining VOC pollutants from the residual layer to the mixing layer after sunrise. Low percentage of ethylene (15.8%) and propylene (9.1%) are also observed in this source which rules out the possible source from

petrochemical sector. Therefore, this factor is likely attributed to plastics industry and its contribution to total VOCs concentration is 10%.

Factor 5 is dominated by single-species isopropylbenzene, accounted for 82.1% in CZ and 80.4% in QT. Isopropylbenzene is used primarily as an intermediate in the production of phenol and acetone. Other usages include the manufacture of styrene, alpha-methylstyrene, acetophenone, detergents and di-isopropylbenzene as a catalyst for acrylic and polyester-type resins; as a thinner for paints, enamels and lacquers; as a solvent for fat and resins; and in printing and rubber manufacture. Therefore, it is attributed to the manufacturing industry for the production of intermediates for a variety products. This source has the smallest contribution to total VOCs concentration at 5%.

Factor 6 is dominated by multiple-species from C9 aromatics, ethylene and propylene; this factor is identified only in QT and XG. High percentage are accounted for 1,2,4-trimethylbenzene (35.3% in QT and 51.8% in XG) and m-ethyltoluene (43.7% in QT and 58.6% in XG), which are key ingredients in industrial chemical processes (Hui et al., 2018; Zhou et al., 2019). Besides, the gradually increasing trend of 1,2,4-trimethylbenzene may be a result of different paints and solvent formulations used to replace the use of toluene and C8 aromatics in printing industry (Shen et al., 2018). This factor also comprises of high percentage of ethylene (37.9% in QT and 47.6% in XG) and propylene (52.4% in QT and 61.5% in XG), which are mainly attributed to petrochemical plants (Mo et al., 2015; Song et al., 2019). Moderate percentage of acetylene, C5 alkanes (i.e. isopentane, 2,2,4-trimethylpentane), C6-8 aromatics (i.e. toluene m,p-xylene, ethylbenzene, benzene) are also accounted in this factor, which are typical product of combustion in iron and steel industry (Tsai et al., 2008). The hourly factor contribution has a clear bimodal peak at 07 and 18 LST, both correspond to industrial activity. Therefore, it is likely attributed to mixed industry not limited to petrochemical industry, printing industry and metal industry. The contribution of mixed industry to total VOC concentration is 21%, which constituted the second largest source of VOC pollution in the study area.

Factor 7 is characterized by benzene, C2-C5 alkanes (i.e. ethane, propane, isopentane), and small proportions of C7-8 aromatics (i.e. toluene, ethylbenzene), which is related to aged air mass (Huang and Hsieh, 2020; Wu et al., 2016).

Ethanes, propane and benzene have low-reaction rates at 0.3, 1.1, and 1.2 (10^{-12} cm^3 $molecule^{-1}$ s^{-1}), respectively, with lifetimes of 23.3, 5.3 and 4.7 days, respectively (Atkinson and Arey, 2003). In addition, this factor is only identified in CZ and its hourly factor contribution mostly existed at more stable levels when compared to other factors except for an obvious peak at 12 LST due to the sea-breeze penetration that pushes the urban polluted aged air mass towards inland area. The ratio between benzene and toluene is often used as indicator of aged air mass. The B/T ratio of this factor is 2.37 which is much higher than vehicle emissions (0.68). Therefore, it is considered to represent the aged air mass and its contribution to total VOCs concentration is 7%.

Factor 8 is characterized by aromatic compounds (i.e. benzene, toluene, xylene isomers (o-xylene, m-xylene and p-xylene), ethyltoluene isomers (i.e. m-ethyltoluene), trimethylbenzene isomers (i.e. 1,2,4-trimethylbenzene)), and fatty groups (ethylene, isobutane, n-butane, and n-hexane) which are related to motorcycle engine exhaust (Jia et al., 2005). This source is only identified in QT and its hourly factor contribution is similar to the vehicle emissions. Therefore, it is considered to represent the motorcycle engine exhaust and its contribution to total VOCs concentration is 7%.

Supplementary figures and tables

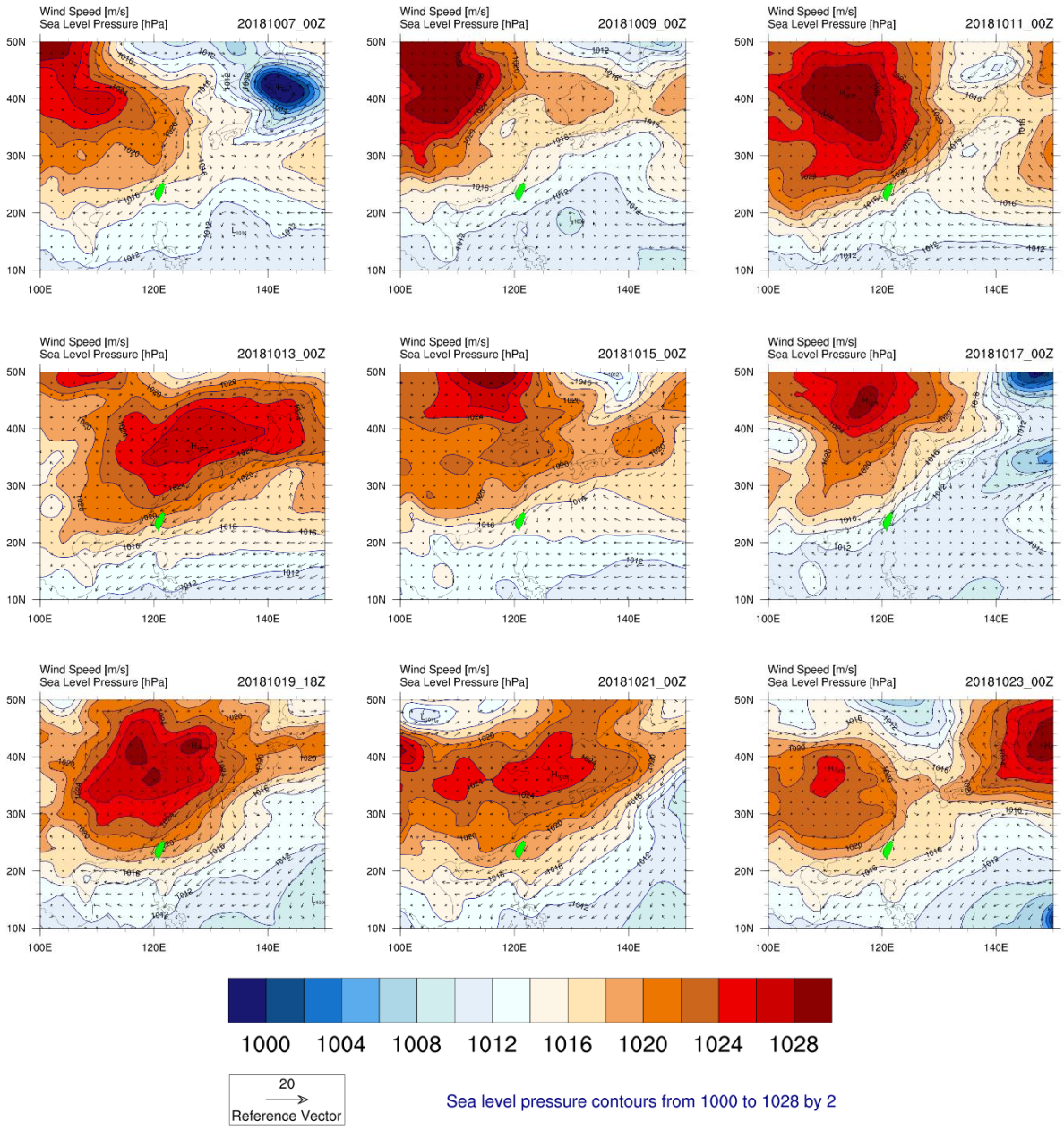

Figure S1: Synoptic weather pattern retrieved from NCEP-FNL reanalysis data valid at 00 UTC from 07 October 2018 to 23 October 2018 showing 850 hPa winds in vector referenced at 20 m s^{-1} and sea level pressure in color contoured from 980 to 1020 hPa by 2 hPa. Taiwan is highlighted with green color.

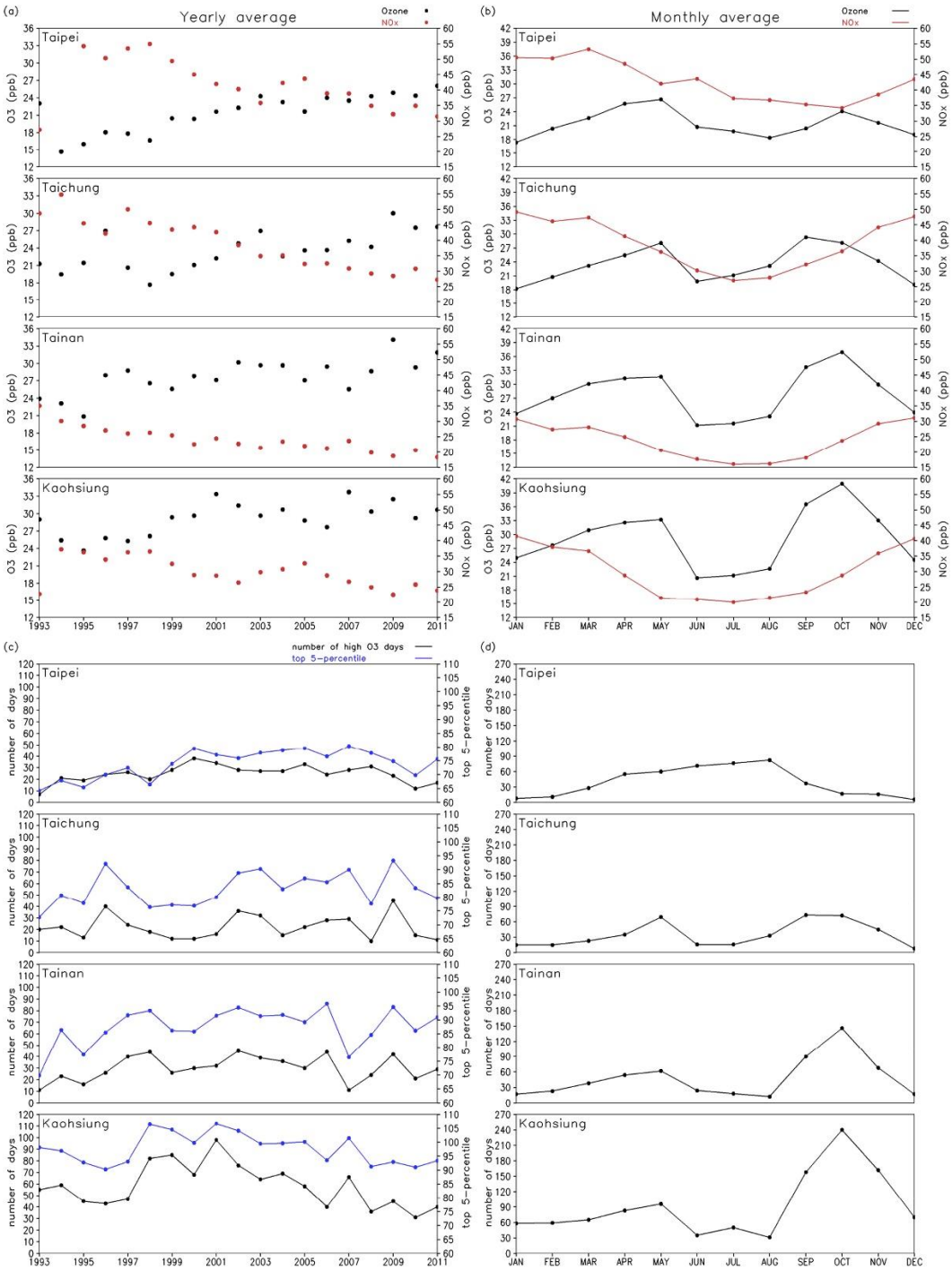

Figure S2. (a) Annual averages of O_3 and NO_x over a 19-year period at the Taipei, Taichung, Tainan and Kaohsiung sites. (b) Same observed data sets as (a) but with O_3 and NO_x presented as monthly variations. (c) Number of high O_3 days (daily maximum O_3 > 100 ppbv) and the average of the top fifth-percentile O_3 concentration in each year. (d) Similar to (c) but presenting the occurrence of days with O_3 > 100 ppbv as monthly variations. Unit for concentrations is in ppbv. Source: (Cheng et al., 2015)

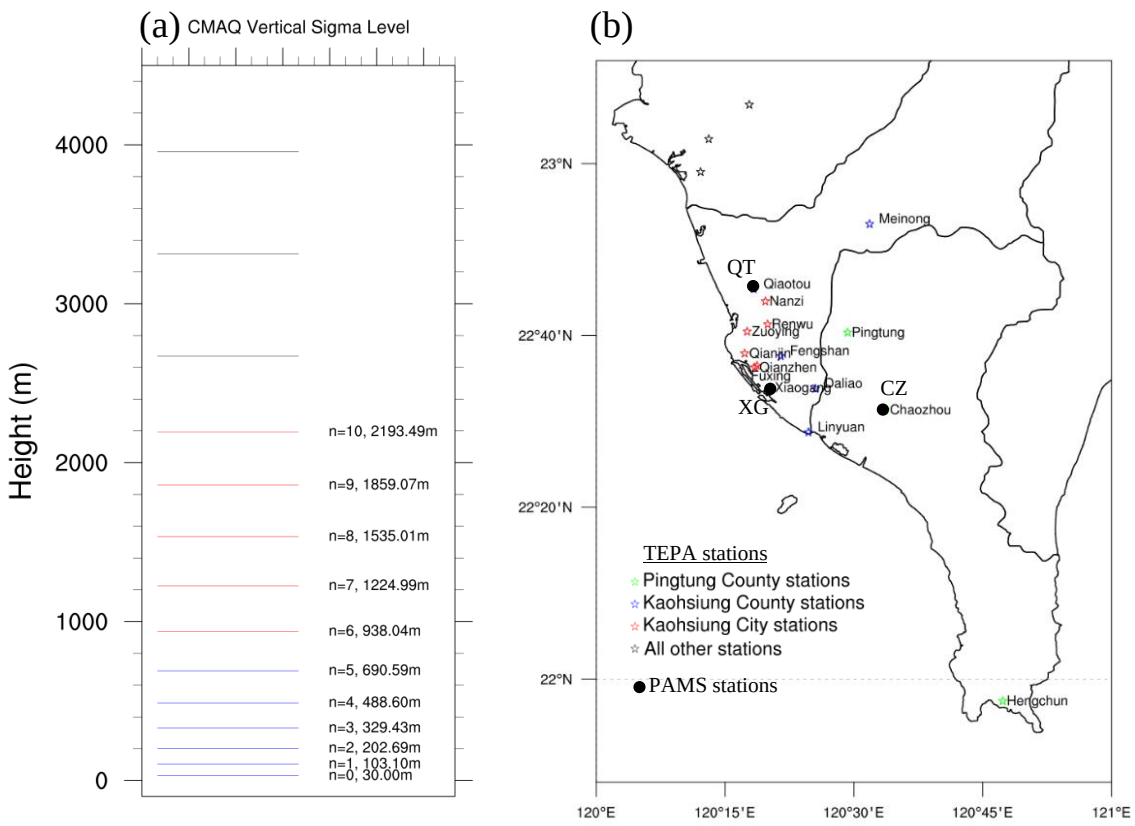

Figure S3: (a) CMAQ vertical layer distribution in eta sigma level. The lowest model level n=0 is approximately 30.0 m above the ground. (b) Distribution of TEPA air quality stations over southern Taiwan.

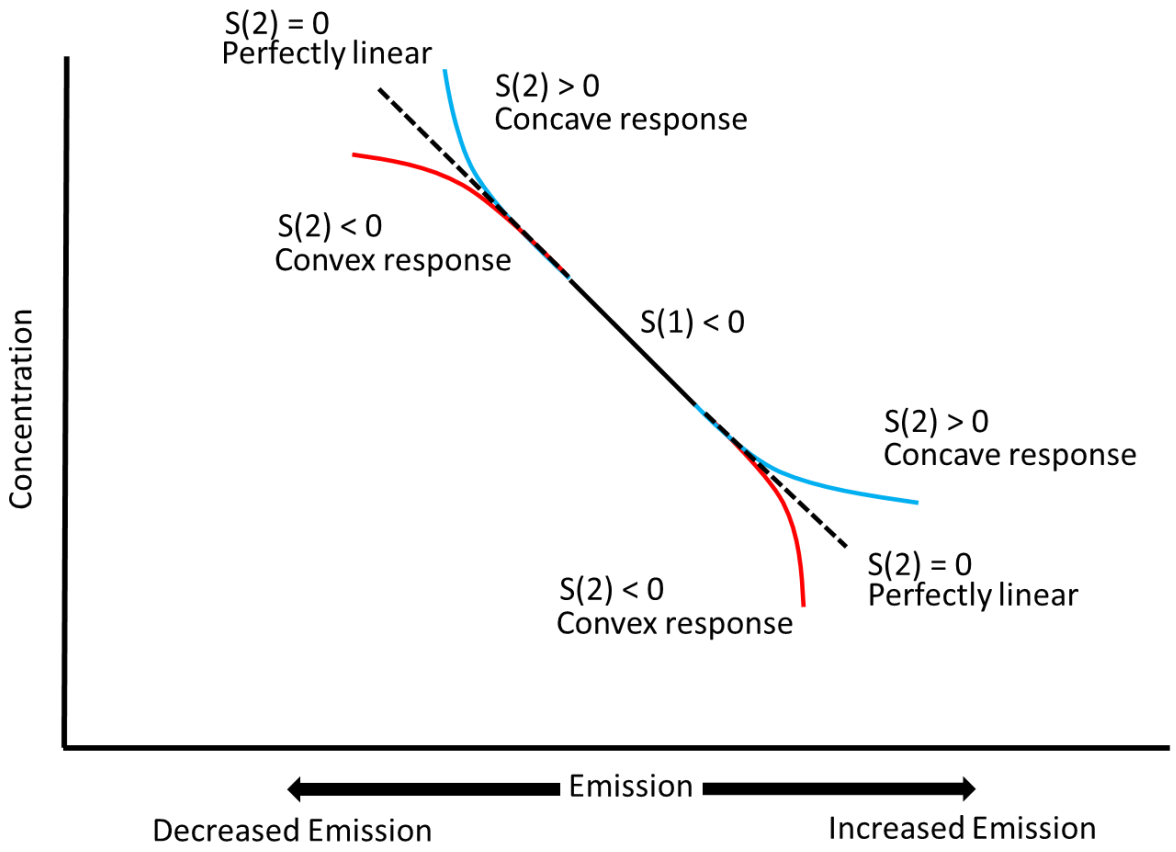

Figure S4: Conceptual diagram of CMAQ-HDDM first-order S(1) and second-order S(2) sensitivity coefficient in convex and concave response.

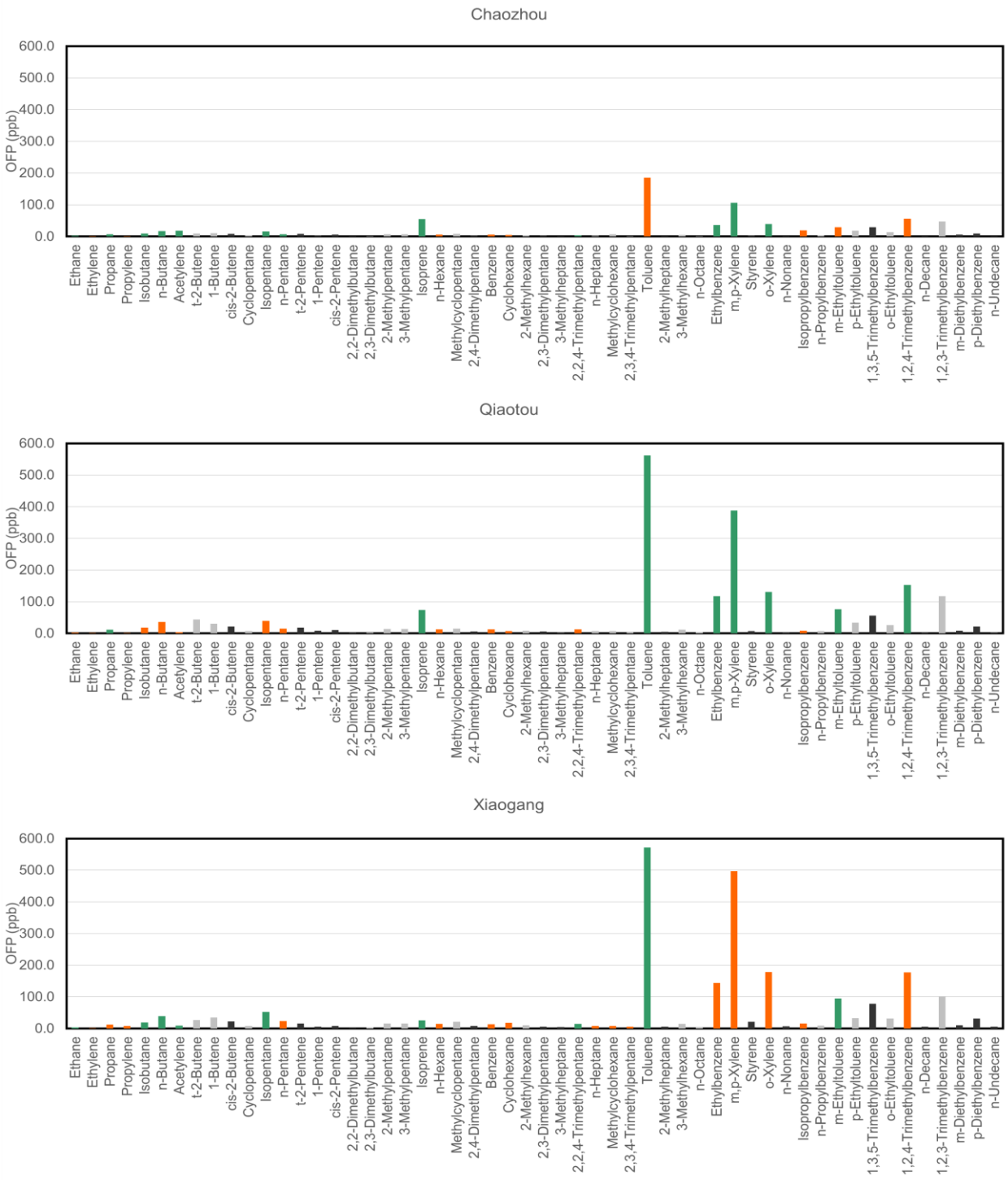

Figure S5: Ozone forming potential (OFP) calculated for each PAMS-VOC species measured at CZ, QT and XG station in Oct 2018. Dark gray species are unused species due to abundant missing data >55% below MDL. Light gray species are poor species with S/N <0.5. Orange (Green) species are weak (strong) species with S/N ≥ 0.5 and R<0.6 (R≥0.6). Both unused and poor species are removed from PMF model analysis.

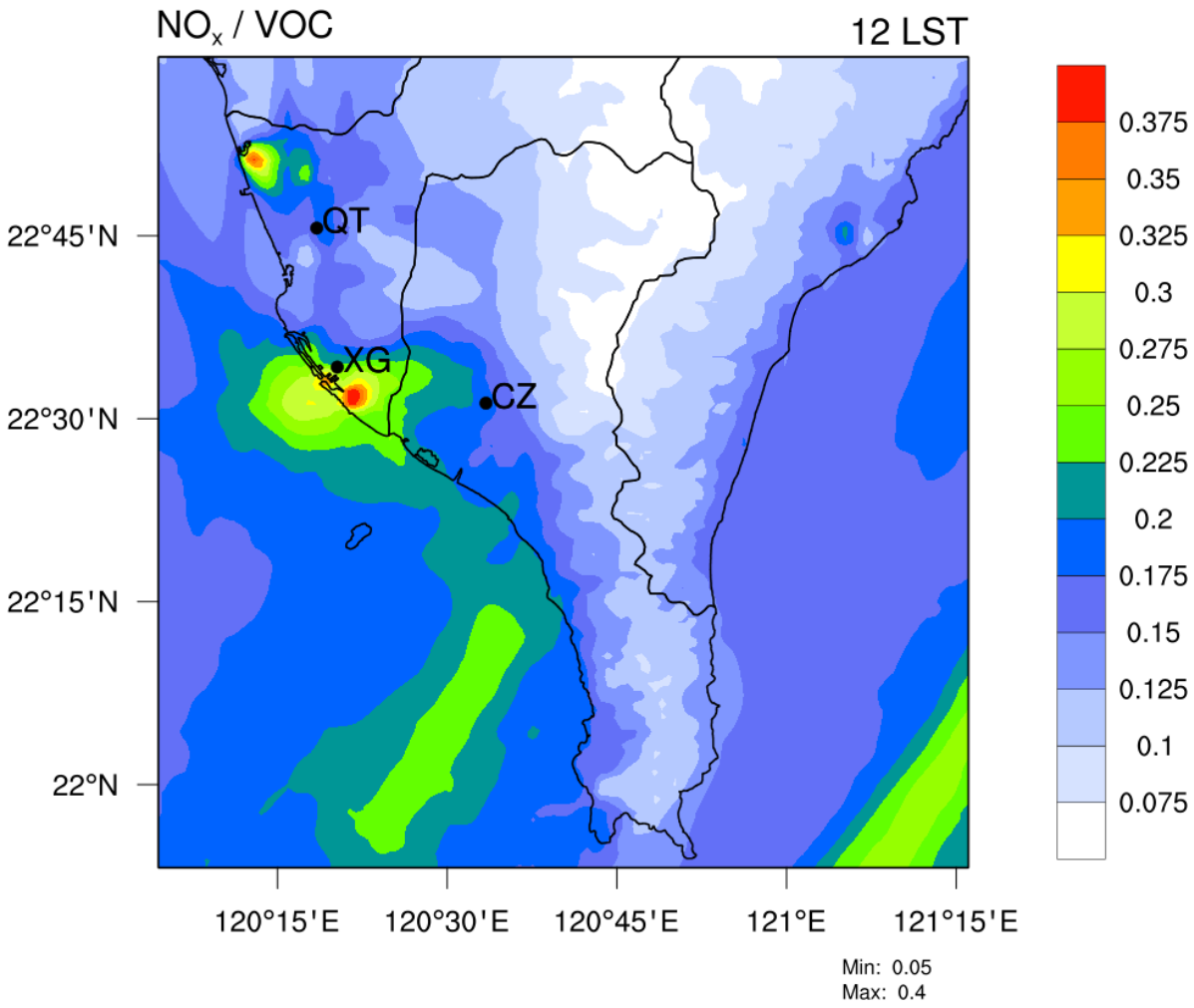

Figure S6: Spatial distribution of ratio NOx / VOC averaged at 12:00 LST during the entire simulation period.

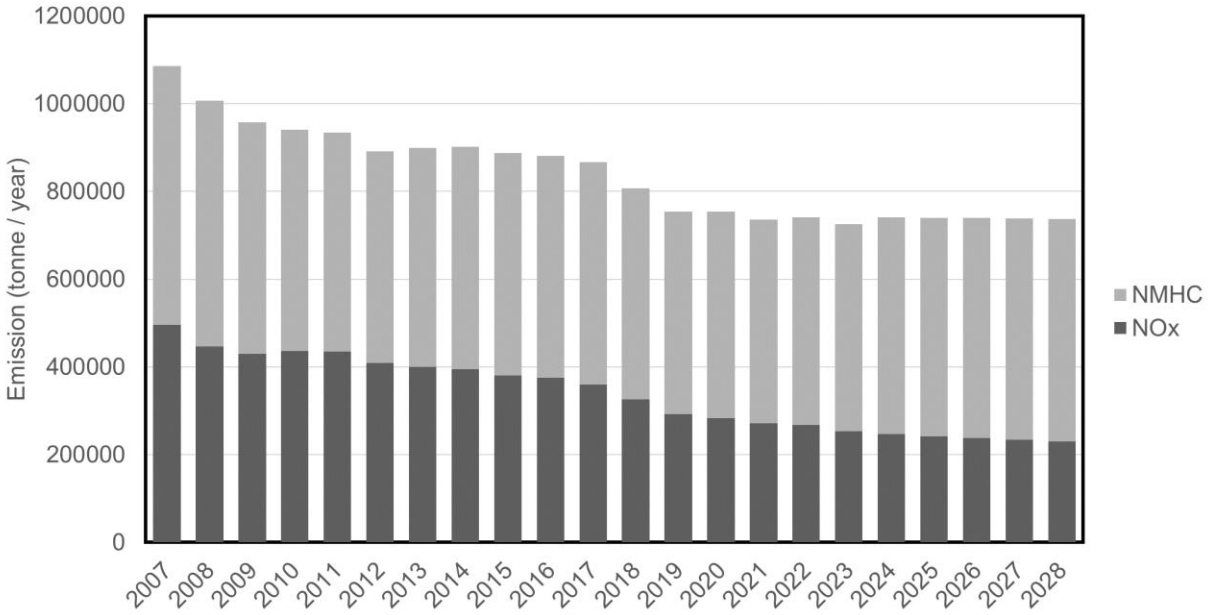

Figure S7: Projected annual emission of NO_x and NMHC in Taiwan from 2007 to 2028 (Source: Taiwan Emission Data System, TEDS 11.0).

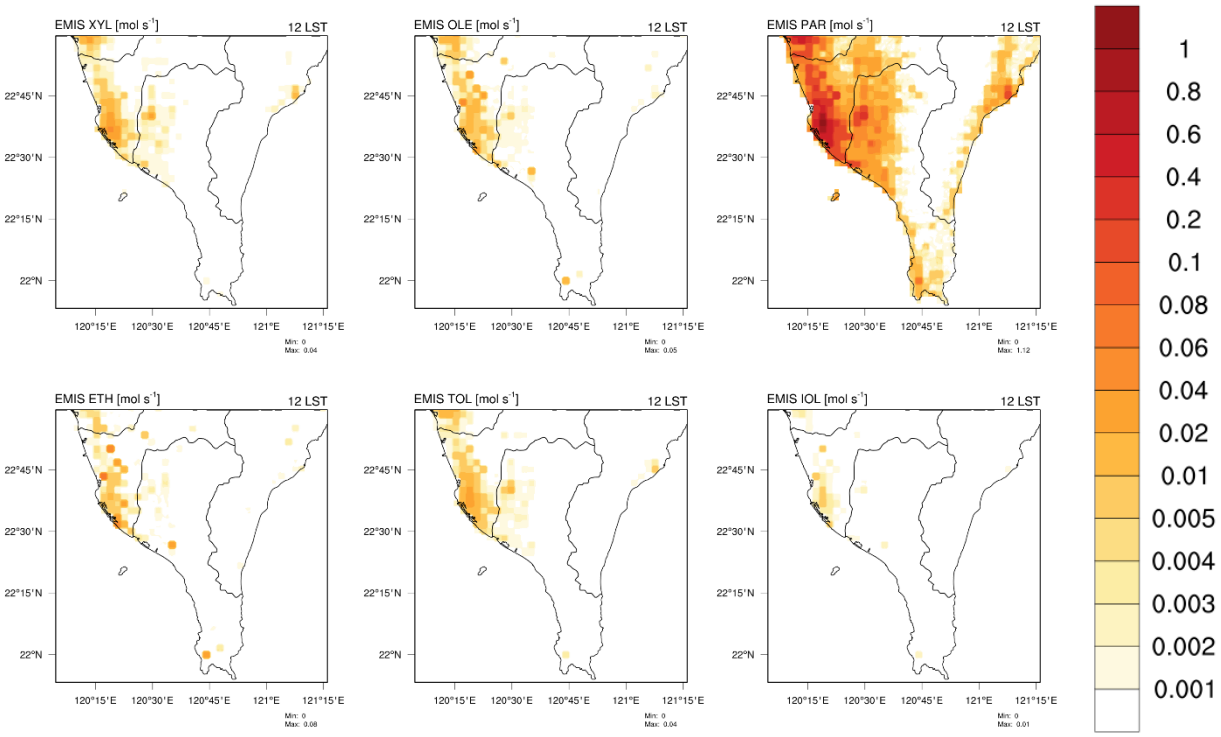

Figure S8: Spatial distribution of some highly sensitive VOC component emissions (i.e. XYL, OLE, PAR, ETH, TOL, IOL) at 12 LST.

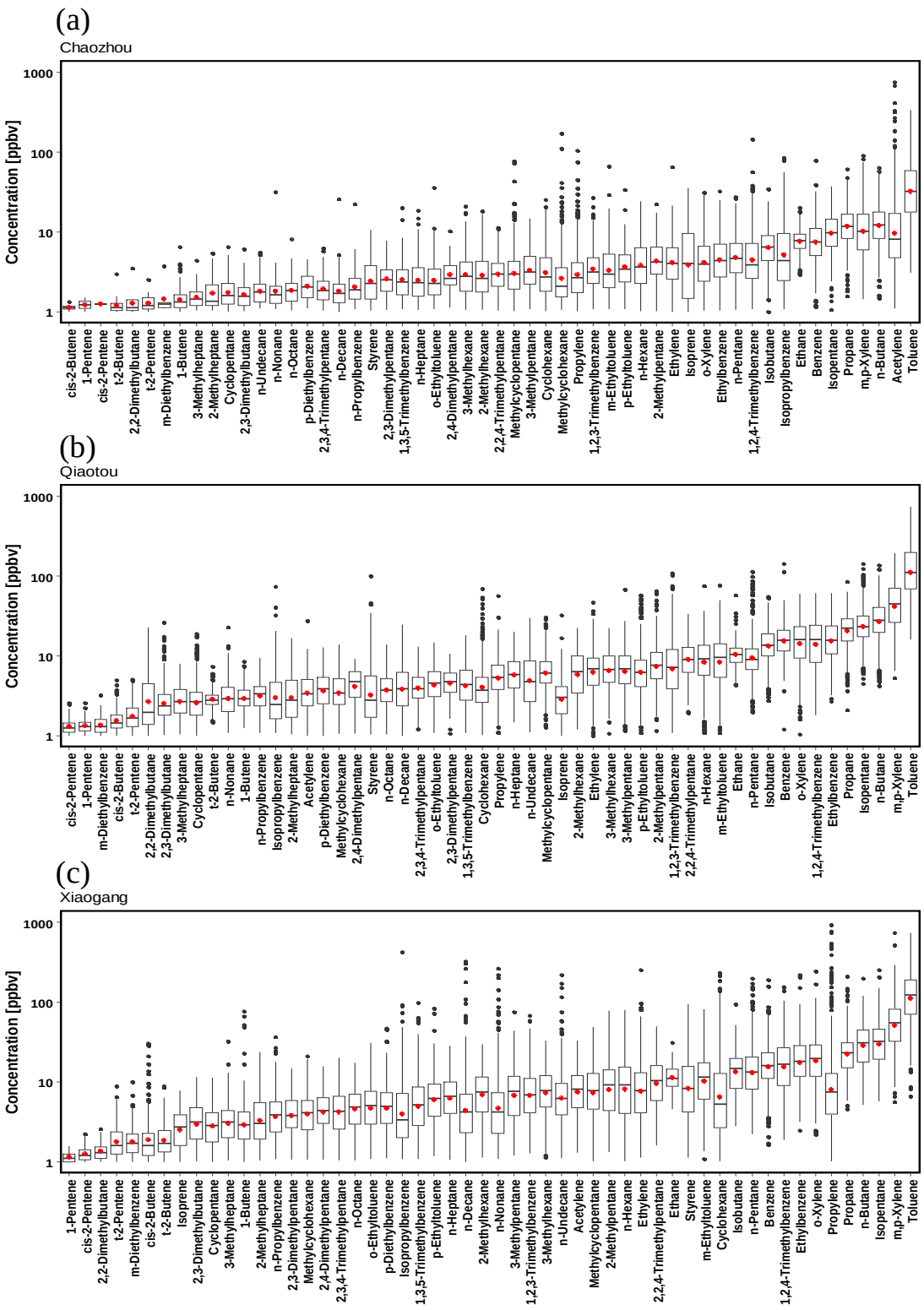

Figure S9: Box plot of 54 PAMS-VOC species measured in (a) Chaozhou, CZ, (b)Qiaotou, QT, (c) Xiaogang, XG during 1-31 October 2018. Species are arranged in ascending order in concentration from left to right.

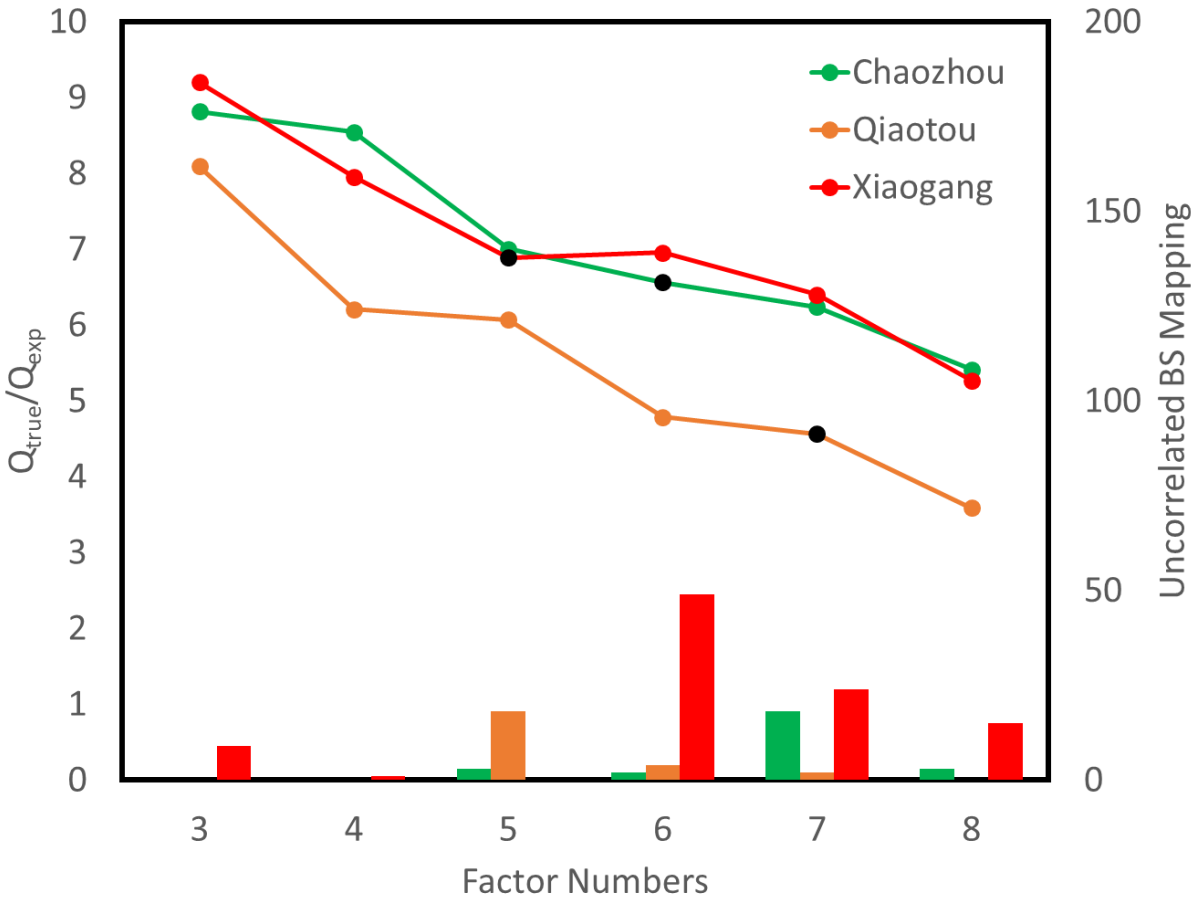

Figure S10: Changes of $Q_{true}/Q_{expected}$ and uncorrelated bootstrap (BS) mapping calculated by the PMF model for increasing factor number from 3 to 8. The black dot represents the optimum solution factors at each station.

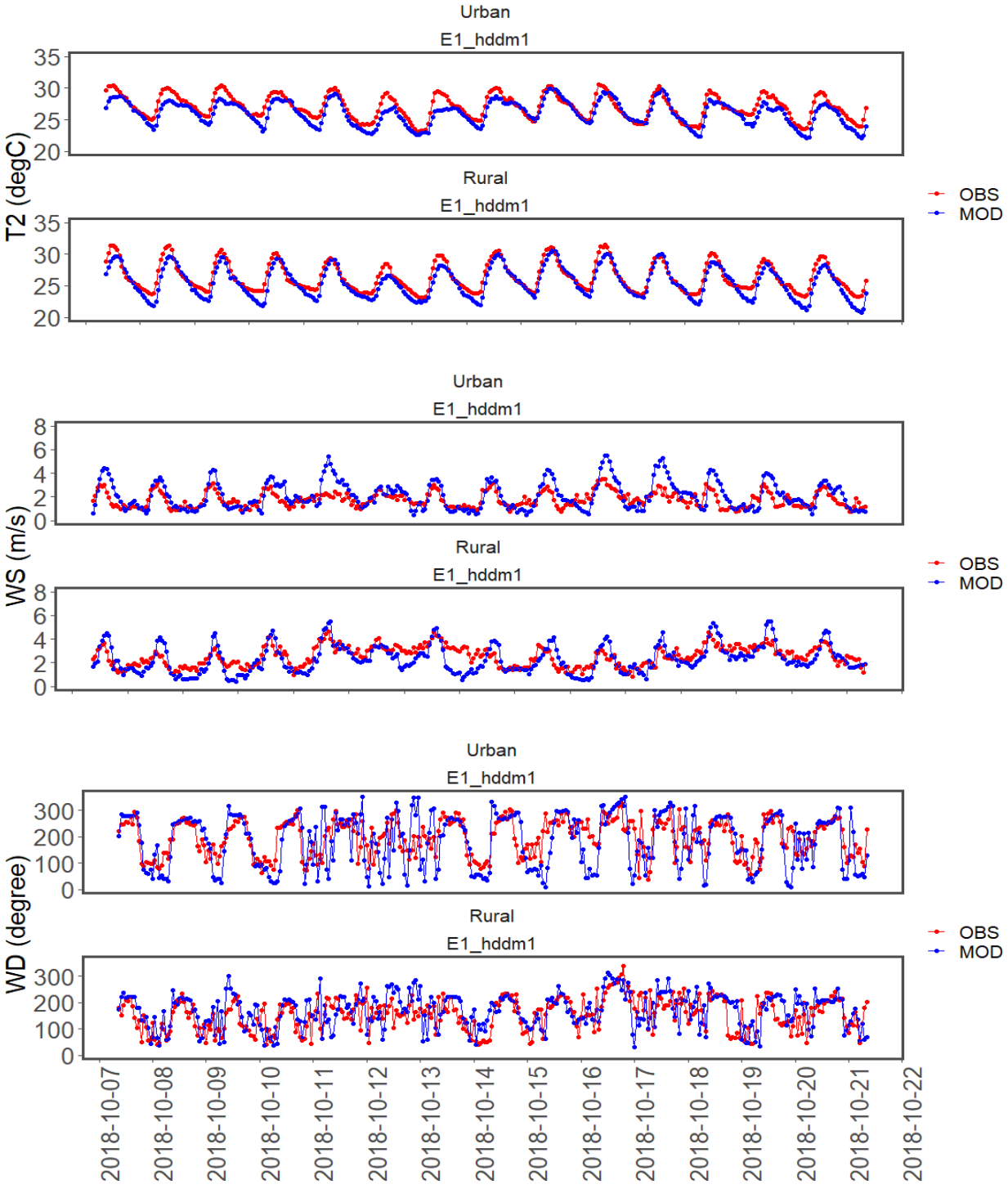

Figure S11: Time series of observed and modelled 2-m temperature (T2), 10-m wind speed and wind direction (WS, WD) averaged over urban (n=10) and rural (n=5) TEPA air quality stations during entire simulation period. Refer Table S3 for urban and rural TEPA air quality stations

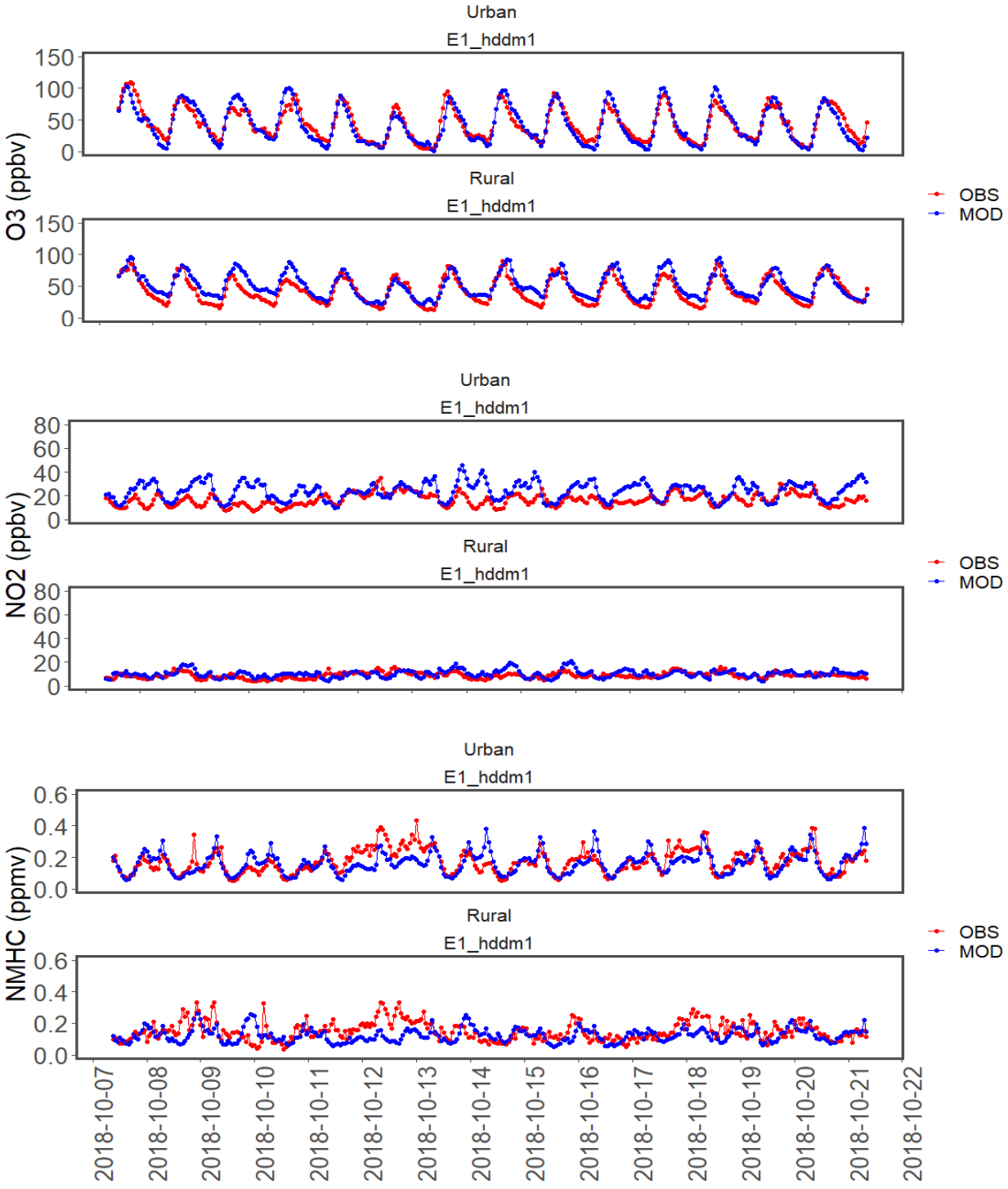

Figure S12: Time series of observed and modelled O_3, NO_2 and VOC averaged over urban (n=10) and rural (n=5) TEPA air quality stations during entire simulation period. Refer Table S3 for urban and rural TEPA air quality stations.

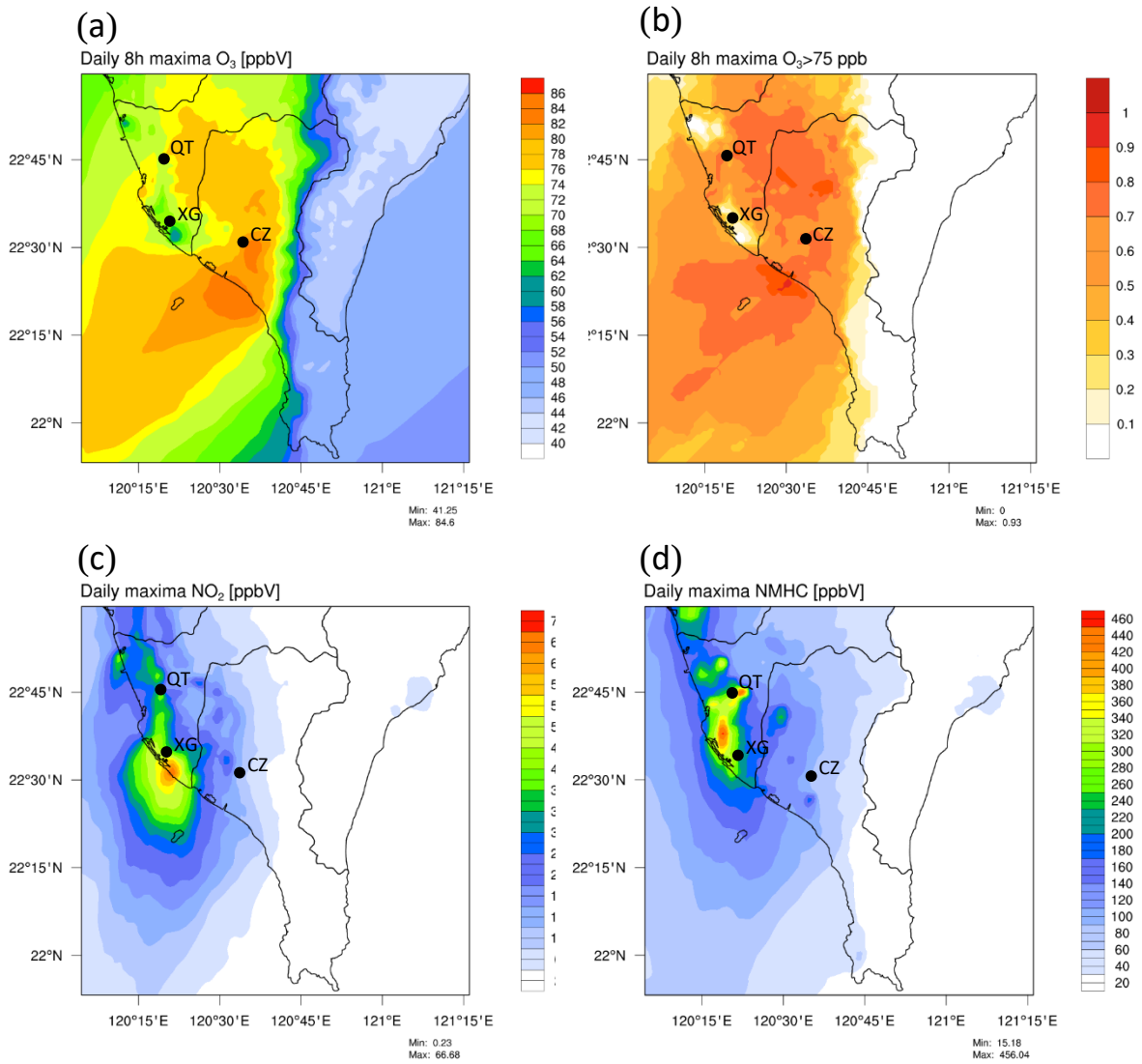

Figure S13: Spatial distribution of (a) daily 8h maxima O_3, (b) occurrence of daily 8h maxima O_3 >75 ppb (c) daily maxima NO_2, (d) daily maxima VOC, averaged during the entire simulation period at the lowest model level in the innermost domain.

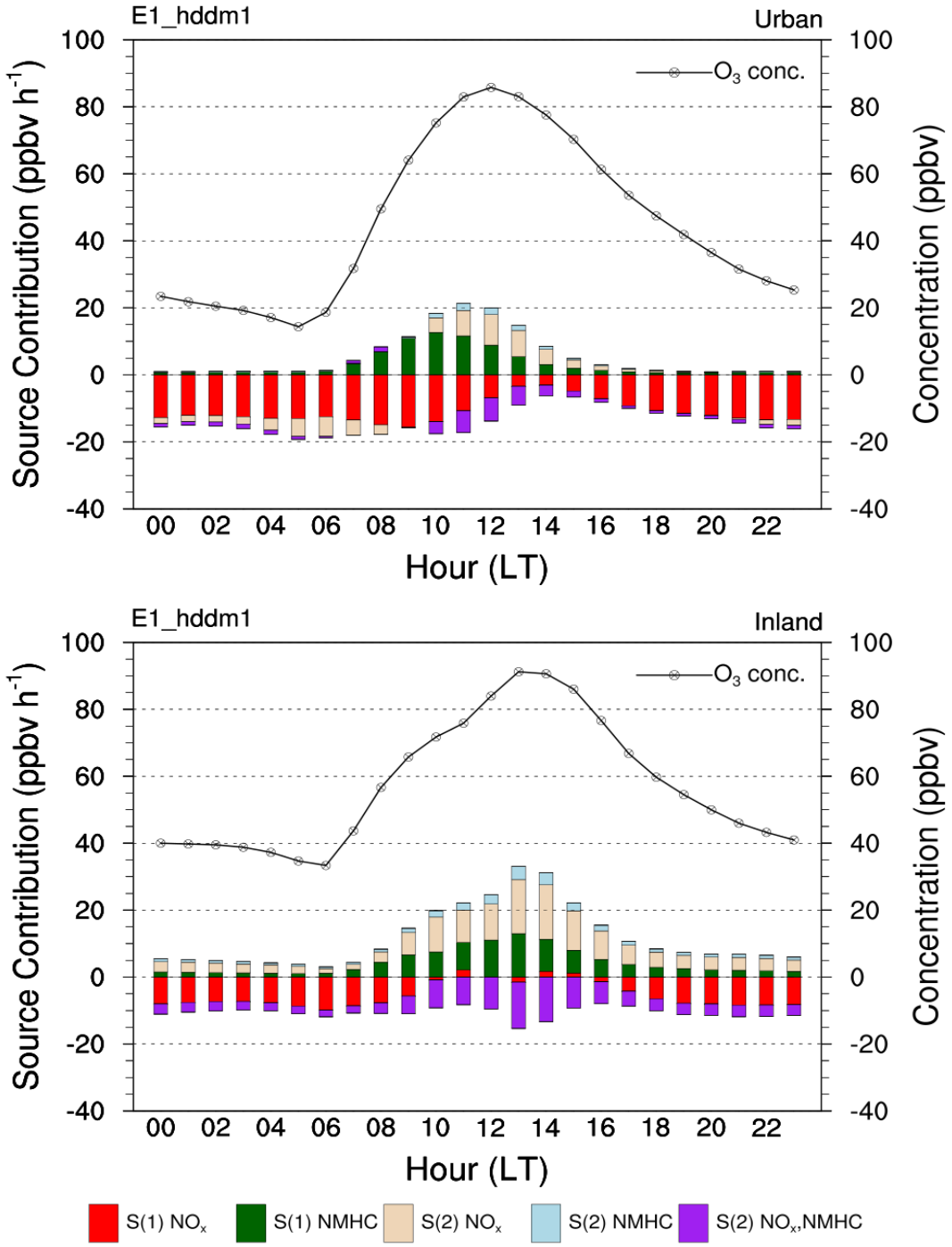

Figure S14: Hourly ozone concentrations (line) and decomposition of the zero-out source contributions of domain-wide NO_x and VOC emissions averaged for (a) urban and (b) inland area, during the entire simulation period. S(1) and S(2) denotes the first-order and second-order sensitivity, respectively; S(2) NO_x,VOC denotes the cross-order sensitivity.

Table S1: Mapping of PAMS-VOC species to CMAQ CB6 modelled VOC species. Oxygenates (FORM, ALD2, ALDX, ACET, KET) and alcohols (ETO, MEOH) are not available in PAMS-VOC species inventory.

		XYL	OLE	PAR	ETH	TOL	IOLE	Oxy FORM	ISOP	Alc ETO	TER	Alc MEO	Oxy ALD2	Oxy ALDX	PRPA	ETHA	NAPH	Oxy ACET	BENZ	Oxy KET	ETHY
alkane	Ethane															M					
alkene	Ethylene				M																
alkane	Propane														M						
alkene	Propylene		M																		
alkane	Isobutane			M																	
alkane	n-Butane			M																	
alkyne	Acetylene																				M
alkane	Isopentane			M																	
alkane	n-Pentane			M																	
isoprene	Isoprene								M												
alkane	n-Hexane			M																	
aromatics	Benzene																		M		
alkane	Cyclohexane			M																	
alkane	2,2,4-Trimethylpentane			M																	
aromatics	Toluene					M															
aromatics	Ethylbenzene																		M		
aromatics	m,p-Xylene	M															M				
aromatics	o-Xylene	M															M				
aromatics	Isopropylbenzene																		M		
aromatics	m-Ethyltoluene					M															
aromatics	1,2,4-Trimethylbenzene																		M		

Table S2: Model evaluation metrics for meteorology (T2, WS, WD, RH) and air quality pollutants (O_3, NO_2, VOC) averaged from 15 TEPA air quality stations during the entire simulation period.

	Meteorology				Pollutants		
	T2	**WS**	**WD**	**RH**	**O_3**	**NO_2**	**VOC**
Unit	°C	ms^{-1}	degree	%	ppbv	ppbv	ppmv
Mean OBS	26.8	2.0	-	77.1	43.6	14.1	0.17
Mean MOD	25.9	2.2	-	70.4	45.2	19.6	0.16
MB	-0.9	0.2	-	-6.7	1.6	5.5	-0.01
MAGE	1.2	1.0	-	7.5	12.5	7.7	0.1
MNB	-3.3	7.6	-	-8.9	2.6	27.9	-0.4
MNE	3.8	44.0	-	9.1	27.1	41.5	35.1
IOA	0.89	0.85	-	0.80	0.91	0.67	0.63
WNMB	-	-	-1.1	-	-	-	-
WNME	-	-	28.3	-	-	-	-

MB: mean bias (±1.5°C, ±1.5ms^{-1}); MNB: mean normalized bias (±15% O_3, -40-50% NO_2 | VOC)
MAGE: mean average gross error (<3.0°C, <3.0ms^{-1}); MNE: mean normalized error (<35% O_3, <80% NO_2 | VOC)
IOA: index of agreement (>0.60)
WNMB: wind normalized mean bias (<±10%); WNME: wind normalized mean error (<30%)

Table S3: Description of 15 TEPA air quality and 3 PAMS stations used in this study

ID	Station	Lon	Lat	Type	Urban/Rural
TEPA1	Zuoying	120.29	22.67	Ambient	Urban
TEPA2	Nanzi	120.33	22.73	Ambient	Urban
TEPA3	Qianjin	120.29	22.63	Ambient	Urban
TEPA4	Xiaogang	120.34	22.57	Ambient	Urban
TEPA5	Linyuan	120.41	22.48	Ambient	Urban
TEPA6	Daliao	120.43	22.56	Ambient	Urban
TEPA7	Renwu	120.33	22.69	Ambient	Urban
TEPA8	Meinong	120.53	22.88	Ambient	Rural
TEPA9	Pingtung	120.49	22.67	Ambient	Rural
TEPA10	Chaozhou	120.56	22.52	Ambient	Rural
TEPA11	Qianzhen	120.31	22.61	Industrial	Urban
TEPA12	Fuxing	120.31	22.61	Traffic	Urban
TEPA13	Fengshan	120.36	22.63	Traffic	Urban
TEPA14	Qiaotou	120.31	22.76	Background	Rural
TEPA15	Hengchun	120.79	21.96	Park	Rural
PAM1	Chaozhou (CZ)	120.56	22.52	-	-
PAM2	Qiaotou (QT)	120.64	22.76	-	-
PAM3	Xiaogang (XG)	120.34	22.57	-	-

Table S4: Episode-averaged of NO_x and VOC emissions (tones per day, tpd), area and emission density by region.

Region	NO_x Emissions (tpd)	Area (km^2)	Emission Density (tpd/km^2)	VOC Emissions (tpd)	Area (km^2)	Emission Density (tpd/km^2)	Reference
Atlanta	536	25168	0.021	-	-	-	(Cohan et al., 2005)
Macon	63	5749	0.011	-	-	-	(Cohan et al., 2005)
Domain	3986	712800	0.006	-	-	-	(Cohan et al., 2005)
Houston	501	21783	0.023	1469	21783	0.067	(Xiao et al., 2010)
Ship Channel	100	320	0.313	108	320	0.338	(Xiao et al., 2010)
Domain	2620	43532	0.060	2140	43532	0.049	(Xiao et al., 2010)
Kaohsiung	723	2835	0.255	-	2835	-	This study
Pingtung	381	2788	0.137	-	2788	-	This study
Urban	807	653	1.236	-	653	-	This study
Inland	187	459	0.407	-	459	-	This study
Domain	1466	14400	0.102	-	14400	-	This study